Journal of Orthopaedic Translation 24 (2020) 209–217

Contents lists available at ScienceDirect

Journal of Orthopaedic Translation

journal homepage: www.journals.elsevier.com/journal-of-orthopaedic-translation

Original Article

Cervical spinal instability causes vertebral microarchitecture change and vertebral endplate lesion in rats

Qi Liu [a,b], Zhou Yang [a], Yapu Liu [a,c], Wei Ji [a], Zucheng Huang [a], Junhao Liu [a], Junyu Lin [a], Yue Hua [d], Zhiping Huang [a], Xiuhua Wu [a], Qingan Zhu [a,*]

[a] Department of Spinal Surgery, Nanfang Hospital, Southern Medical University, Guangzhou, PR China
[b] Department of Orthopaedic Surgery, The Second Affiliated Hospital of Guangzhou Medical University, PR China
[c] Department of Spinal Surgery, The Second Affiliated Hospital of Luohe Medical College, Luohe, Henan, PR China
[d] School of Traditional Chinese Medicine, Southern Medical University, Guangzhou, PR China

ARTICLE INFO

Keywords:
Biomechanical property
Bone formation
Intervertebral disc degeneration
Spinal instability
Vertebral endplate damage

ABSTRACT

Background: The vertebral endplate (VEP) was damaged after spinal instability induced by cervical muscle section (CMS). Whether CMS induces bone formation and mechanical loading change in the vertebra is still obscure. This study was aimed to explore mechanical loading change and endplate damage after CMS.

Methods: Forty-eight rats were randomly divided into the CMS group and the sham group. The C6/7 segments were harvested at 4, 8, and 12 weeks after surgery. The microarchitectures of the C6 vertebra and the vertebral endplate lesions and intervertebral disc height of C6/7 were measured by micro–computed tomography. Micro–finite element analysis was used to evaluate biomechanical properties of the C6 vertebra. Bone remodelling of the C6 vertebra and the endplate sclerosis and intervertebral disc degeneration of C6/7 were evaluated by histological and immunohistochemical analyses.

Results: CMS significantly induced bone formation of the C6 ventral vertebra and increased the biomechanical properties of mainly the ventral side at 4 weeks, which was gradually rebalanced throughout the rest of the study. CMS also significantly increased protein expression of transforming growth factor-β1 (TGF-β1) and phosphorylated small mothers against decapentaplegic (pSmad)2/3 at 4 weeks. Moreover, tartrate-resistant acid phosphatase staining showed that osteoclast-positive cells were slightly in number decreased at 4 weeks, but were obviously increased at 8 weeks. The VEP of the ventral side was abraded earlier followed by calcification in situ later after CMS, consistent with the biomechanical enhancements observed. The degree of endplate degeneration was aggravated with time. Finally, CMS decreased intervertebral disc height and increased disc degeneration scores with time.

Conclusions: Spinal instability induced by CMS increases bone mass and biomechanical loading of the ventral side of vertebra in the early stage, which might initiate VEP damage and cause intervertebral disc degeneration.

The translational potential of this article: Our study indicates that vertebral trabecular changes may involve in intervertebral disc degeneration induced by spinal instability. This may help to elucidate the mechanisms by which disc degeneration occur.

Introduction

Intervertebral disc degeneration (IVDD) is one of the most common musculoskeletal disorders, which has a significant impact on patients' quality of life and increases the social economic burden [1–3]. Several factors, including ageing [4], metabolic disorders [5], and mechanical factors [6], have been implicated to cause IVDD. However, the initiation pathogenic factor of IVDD is still under debate.

Intervertebral disc is composed of three distinct components: the central gelatinous nucleus pulposus (NP), the outer annulus fibrosus (AF), and the vertebral endplate (VEP) that anchors onto the vertebral body [7]. As the chondroid tissue, the VEP transfers not only the load between vertebrae but also nutrients between vertebral body and disc [8]. Endplate sclerosis changes the mechanical properties and impairs nutrient supply to the NP, thus might initiate IVDD [9]. The subchondral bone of joints provides the mechanical support for the overlying articular

* Corresponding author. Department of Spinal Surgery, Nanfang Hospital, Southern Medical University, Guangzhou, PR China.
E-mail address: qinganzhu@gmail.com (Q. Zhu).

https://doi.org/10.1016/j.jot.2019.10.005
Received 9 July 2019; Received in revised form 11 October 2019; Accepted 14 October 2019
Available online 6 November 2019

cartilage during movement and undergoes constant adaptation in the mechanical environment through modelling or remodelling [10]. As the similar structure of the subchondral bone in the joint, the vertebra in spine might also play an important role for maintaining disc homoeostasis.

The spine is inherently unstable and must be stabilised by a combination of muscular and spinal structures [11]. The stable intradiscal pressure is essential for the maintenance of biomechanical behaviours of the intervertebral disc, and appropriate mechanical loading produced by body weight and muscle force is necessary to regulate endplate property and NP anabolic activity [12]. It is known that the disturbance of stress distribution generates stress concentration which increases the risk of VEP fracture [13], and the abnormal biomechanics has long thought to be a major aetiology of IVDD [6,14]. Forelimb amputation in rats upregulated TGF-β in vertebra and VEP, which resulted in bone formation of the vertebra and caused calcified hypertrophy of VEP [15,16]. Similarly, our previous study also found that cervical spinal instability induced by bilateral facetectomy led to earlier bone formation in the vertebra [17]. In addition, instability of cervical spine induced by cervical muscle section (CMS) causes noticeable VEP damage in the ventral side and IVDD [18,19]. However, the spatiotemporal bone formation and vertebral biomechanical enhancement of the ventral side after CMS is still ambiguous.

Therefore, the aim of this study was to investigate the changes of vertebral microarchitectures and vertebral biomechanical loadings in the ventral and dorsal parts, as well as the VEP damage and IVDD in the CMS rats. We hypothesised that (1) instability of cervical spine induced by CMS caused bone remodelling in the ventral vertebra in the early phase and (2) the bone remodelling in the ventral vertebra significantly increased with the vertebral biomechanical loading at 4 weeks, and (3) the elevated biomechanical loading initiated the VEP damage and IVDD.

Materials and methods

Animal model and specimen preparation

Forty-eight male Sprague–Dawley rats (weighing from 230 g to 250 g) were purchased from Experimental Animal Center of Southern Medical University. After 3 days of adaptation, the rats were randomly divided into the CMS group and the sham group. After anaesthesia by a mixture of O_2/isoflurane (1–4%), transection of the paraspinal musculature and the posterior cervical spinal ligaments from C2 to C7 was performed in the CMS rats to induce cervical spinal instability, while the sham animals only underwent skin incision. All rats were kept in the rat's cage with a 12-h light–dark cycle, and a constant temperature of 25 °C and 48% humidity level. This study was approved by the Animal Center of Southern Medical University, and all animal experiments were approved and performed in accordance with the guidance made by the Animal Ethics Committee of Southern Medical University.

After euthanised with an overdose of 3% pentobarbitone sodium, the C6/7 segments of the rats were harvested at 4, 8, and 12 weeks after surgery. The soft tissues of C6/7 segments were carefully removed, and then fixed in 4% paraformaldehyde for 48 h before micro–computed tomography (micro-CT) scan, histological and immunohistochemical analyses.

Micro-CT scan

To investigate the bone microstructures of the C6 vertebra, the intervertebral disc height (IDH) of C6/7, and the vertebral endplate volumes (VEV) and vertebral endplate lesions (VEL) of C6/7, the samples were scanned by high-resolution micro-CT (μCT 80; Scanco Medical AG, Switzerland). Each specimen was washed with tap water for 2 h before being scanned by micro-CT with an isotropic voxel size of 15 μm (55 kV, 145 μA, integration time 400 ms, averaged 2 times).

Total cancellous bone of the C6 vertebral body, together with the ventral and dorsal side of the C6 vertebra, was selected for three-dimensional trabecular analysis. The ventral and dorsal vertebrae were distinguished by the midperpendicular of vertebral width of ventral to dorsal in the transverse plane. Microstructures of cancellous bone were characterised using standardised techniques to determine the bone volume fraction (bone volume/total volume, BV/TV), the trabecular thickness (Tb.Th), the trabecular number (Tb.N), and the trabecular separation (Tb.Sp). The IDH of C6/7 was measured as the distance between the ventral–dorsal midpoints of C6 caudal and C7 cephalic endplates in the midsagittal section. Image Processing Language software (version 5.15; Scanco Medical AG, Switzerland) and Image-Pro Plus image analysis software (version 6.0; Media Cybernetics, Inc., Rockville, MD, USA) were used to evaluate VEL of C6 caudal and C7 cephalic endplates [18]. The VEV of C6 caudal and C7 cephalic endplates was defined to cover visible bony plate close to the vertebra.

Micro–finite element analysis

Biomechanical properties of the entire C6 vertebra, together with the ventral and dorsal vertebrae, were assessed by micro–finite element analysis (micro-FEA). The micro-FEA software (version 1.13; Scanco Medical AG) is an addition to the Image Processing Language software delivered by Scanco for image manipulation and enhancement. The software addition involves a set of functions that enables finite element analysis of structures as represented by three-dimensional micro-CT images. For the micro-FE model, linear elastic material properties were prescribed for the voxels representing bone tissue, with a Young's modulus of 10 GPa and a Poisson's ratio of 0.3. Boundary conditions represented 'high-friction' compression tests to a compressive strain of 1%. The stiffness of the sample was derived as the ratio of the calculated reaction force at 1% compression over the prescribed displacement. The failure load was estimated as the external force for which the von Mises stress exceeds 70 MPa for more than 2% of the bone tissue.

Histological evaluation

After being scanned by micro-CT, the C6/7 samples were decalcified in 10% ethylene diamine tetraacetic acid (EDTA) for 4–5 weeks. The specimens were embedded in paraffin after being washed overnight in deionised water. The blocks were cut into 5-μm-thick sections, and the histological examination was performed by haematoxylin–eosin and safranin O/fast green staining to observe the bone histomorphology and the degeneration of VEP and interverbral disc. The extent of IVDD was assessed by a disc degeneration assessment scoring system [20].

Immunohistochemical observation

All the sections were deparaffinized in xylene and rehydrated with a reverse-graded series of ethanol, followed by incubation in 3% H_2O_2 for 30 min to block endogenous peroxidase activity. After antigen retrieval, all the slices were subsequently incubated overnight with primary antibodies against TGF-β1, pSmad2/3, and Col I (1:100, ANBO Biotechnology Co., Ltd., SF, USA) at 4 °C in a humidified chamber. After a thorough wash, each section was incubated with biotinylated goat anti–rabbit-IgG (Boster Corporation, Wuhan, China) and Streptavidin–horse radish peroxidase (HRP) (Boster Corporation, Wuhan, China), both at room temperature for 30 min. The sections were developed with 3′3-diaminobenzidine until the appropriate stain intensity was obtained. The tartrate-resistant acid phosphatase (TRAP) staining was performed using a standard protocol (Jiancheng, Nanjing, China). Quantitation of TGF-β1, pSmad2/3, and TRAP was conducted in a blinded fashion with Image-Pro Plus Software. The positive cells were obtained by counting the number of positive staining cells in the whole of vertebra.

Statistical analysis

All data were expressed as mean ± standard deviation and were

analysed by Statistical Package for the Social Sciences, version 20.0 (SPSS Inc, Chicago, IL). The independent sample *t* test was performed to determine statistical significance of the microstructure indices of the C6 vertebra, the biomechanical parameters, the IDH, the VEV and the VEL, and quantification of the immunohistochemical staining at each time point. The two-factor analysis of variance was used to determine the effect of CMS on biomechanical parameters in the ventral and dorsal vertebra. The Mann–Whitney nonparametric *U* test was used to analysis the histological scores of intervertebral disc and VEP degeneration. The level of significance was set at $P < 0.05$.

Results

CMS induces bone formation in the C6 vertebra at an early stage

Micro-CT results indicated a dramatic increase in the bone volume of the C6 vertebra in the CMS group compared with that in the sham group in the early stage. The BV/TV, Tb.N, and Tb.Th were significantly higher in the CMS group than those in the sham group (CMS vs. sham: 51.0% vs. 45.4%, 4.40 mm^{-1} vs. 3.84 mm^{-1}, and 117.2 μm vs. 100.8 μm, respectively; $P < 0.05$) at 4 weeks. Meanwhile, the Tb.Sp was significantly decreased after CMS surgery (CMS vs. sham: 187.2 μm vs. 209.5 μm; $P < 0.05$). Interestingly, these changes showed no difference between the CMS and sham groups at the time points of 8 and 12 weeks (Figure 1A and B). In addition, we found that bone formation mainly occurred in the ventral side of the C6 vertebra at 4 weeks (Figure 2A). The BV/TV, Tb.N, and Tb.Th in the ventral vertebra were increased by 22.9%, 15.5%, and 26.5%, respectively, whereas the Tb.Sp was decreased by 19.4% in the CMS group compared with that in the sham group at 4 weeks after surgery (Figure 2B). There was no significant difference between the CMS and sham groups in the bone microstructures of the dorsal vertebra (Figure 2C).

Furthermore, the haematoxylin–eosin and Col I staining were also confirmed that CMS induced early bone formation in the C6 vertebra at the early stage (Figure 1C and D). The bone trabecula was overtly increased and the expression of Col I was significantly enhanced at 4 weeks after surgery in the CMS group compared with the sham group, while showing no difference between groups at 8 and 12 weeks after surgery.

To observe bone remodelling in C6 vertebra, the staining of TGF-β1 and pSmad2/3, which are markers of bone formation, and TRAP, which represents the osteoclast activity, were performed. We found that CMS significantly increased the expression of TGF-β1 (1.57 folds in the CMS group vs. the sham group) and pSmad2/3 (1.55 folds in the CMS group vs. the sham group) at 4 weeks after surgery. The process of bone formation tended to balance at the time of 8 and 12 weeks. On the other hand, TRAP staining showed that osteoclast-positive cells were slightly decreased in number (0.45 fold in the CMS group compared with sham group) at 4 weeks but were obviously increased (2.18 folds in the CMS group vs. sham group) at 8 weeks. Finally, TRAP-positive cells returned to normal level at the time of 12 weeks (Figure 3).

CMS increases the biomechanical properties of the C6 vertebra in the ventral side in the early phase

Micro-FEA data showed that CMS augmented biomechanical properties in the C6 vertebra by increasing the stiffness (CMS vs. sham: 5403.4 N/mm vs. 8446.5 N/mm, $P = 0.036$) and the failure load (CMS

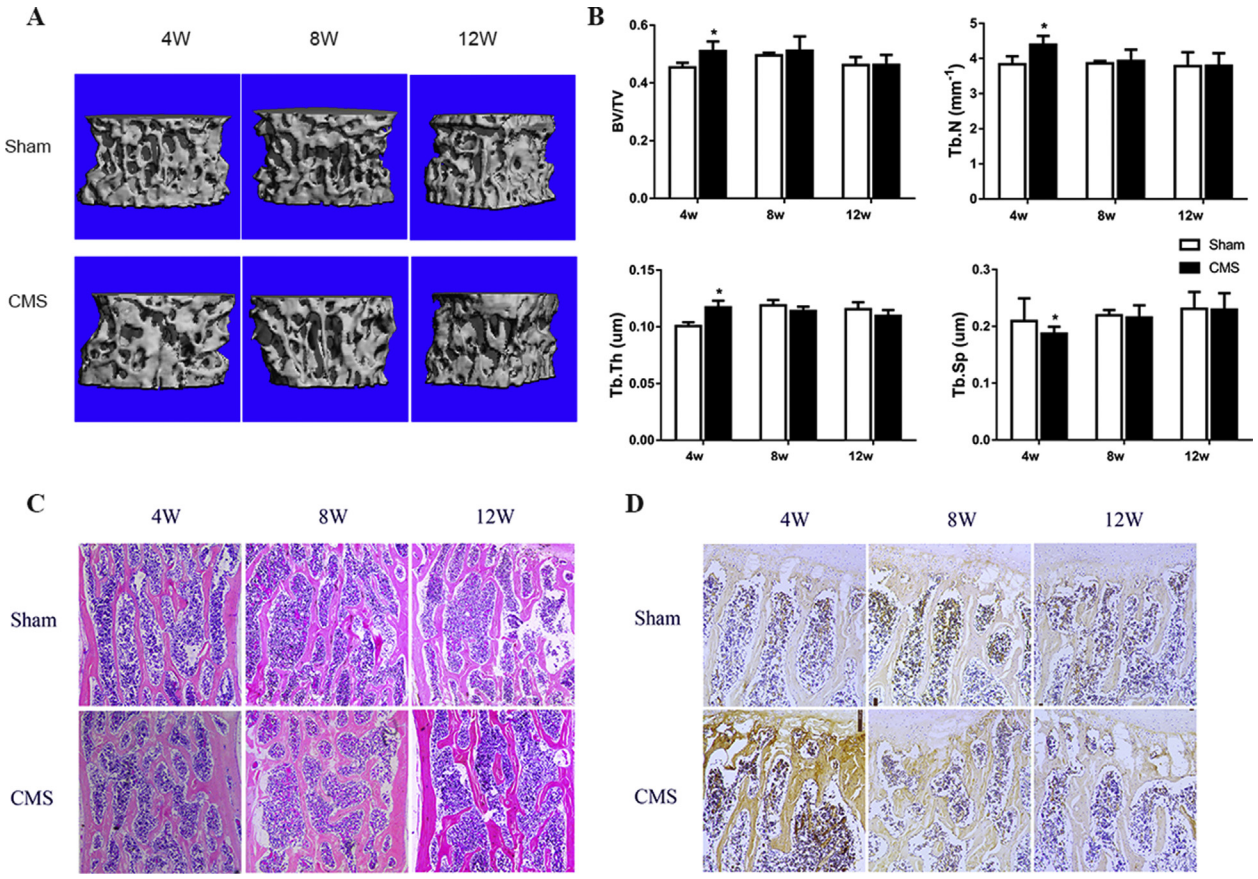

Figure 1. A-D) CMS-induced bone formation in the C6 vertebra at early stage. (A) The three-dimensional reconstructive images of the C6 vertebra. (B) The microstructure analysis of cancellous bone at the C6 vertebra, CMS significantly increased the BV/TV, Tb.N, and Tb.Th, whereas decreased the Tb.Sp at 4 weeks. (C, D) Representative HE staining and Col I staining in the C6 vertebra. All data were shown as mean ± SD (n = 8). "*" indicated $P < 0.05$ compared with the sham group. BV/TV = bone volume fraction; Tb.N = trabecular number; Tb.Th = trabecular thickness; Tb.Sp = trabecular separation; HE staining = haematoxylin–eosin staining.

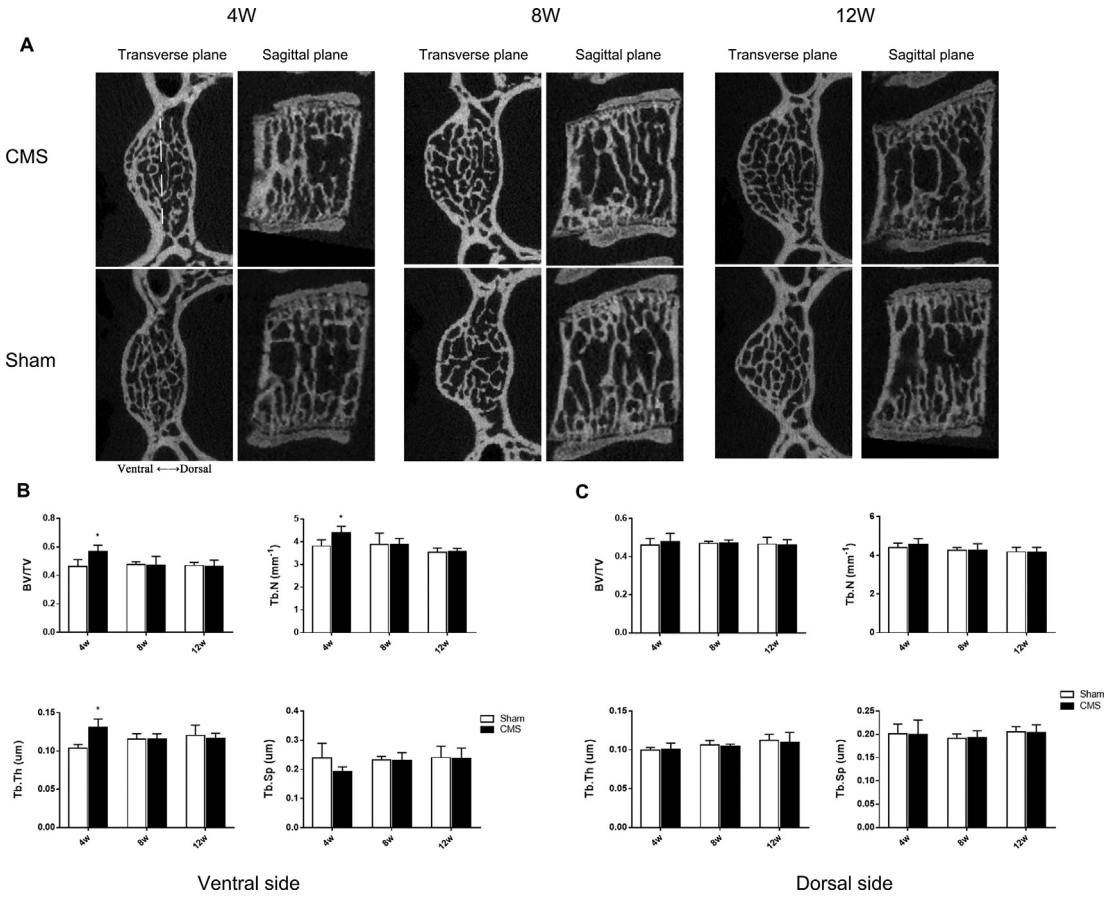

Figure 2. A–C) The bone formation of the ventral and dorsal sides in the C6 vertebra. (A) The transverse and sagittal planes of the C6 vertebra. The yellow dotted line means the midperpendicular of vertebral width of ventral to dorsal in the transverse plane to distinguish the ventral and dorsal side (showed in upper left corner image). (B, C) The microstructure parameters of cancellous bone of the C6 vertebra in the ventral and dorsal sides. "*" indicated $P < 0.05$ compared with the sham group.

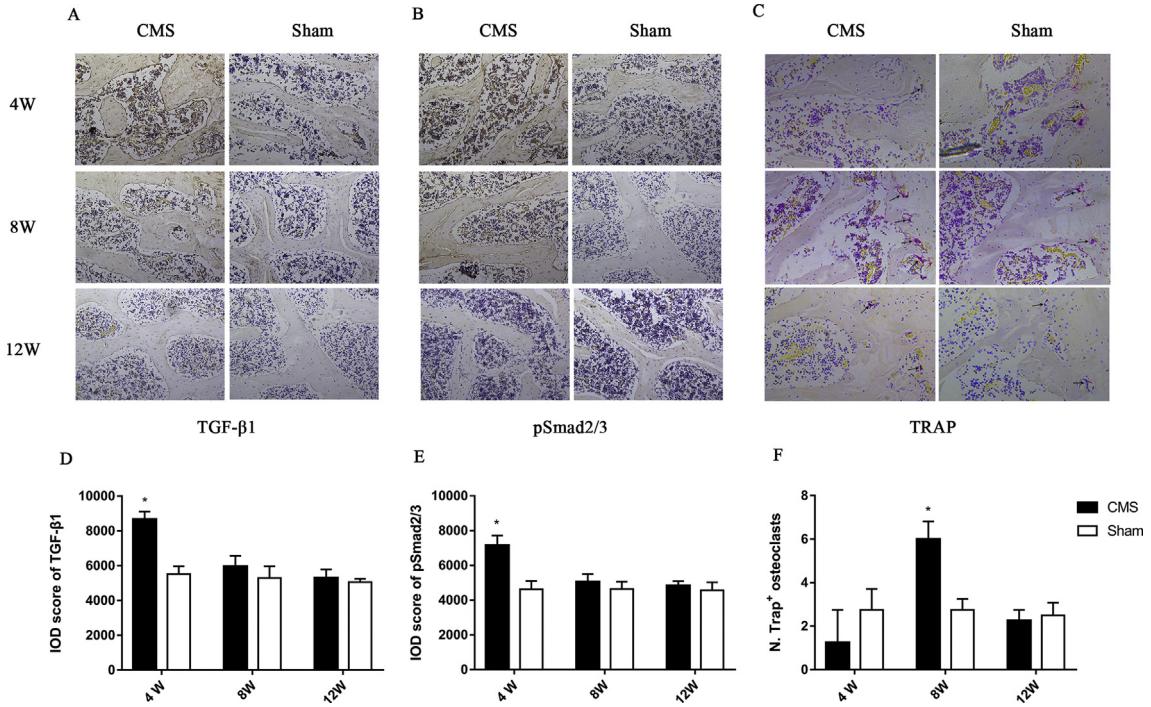

Figure 3. A-F) The immunohistochemistry staining of bone remodelling. (A, B, and C) The staining of TGF-β1, pSmad2/3, and TRAP in the C6 vertebra. (D, E, and F) Quantitation of the staining of TGF-β1, pSmad2/3, and TRAP. "*" indicated $P < 0.05$ compared with the sham group. TRAP = tartrate-resistant acid phosphatase.

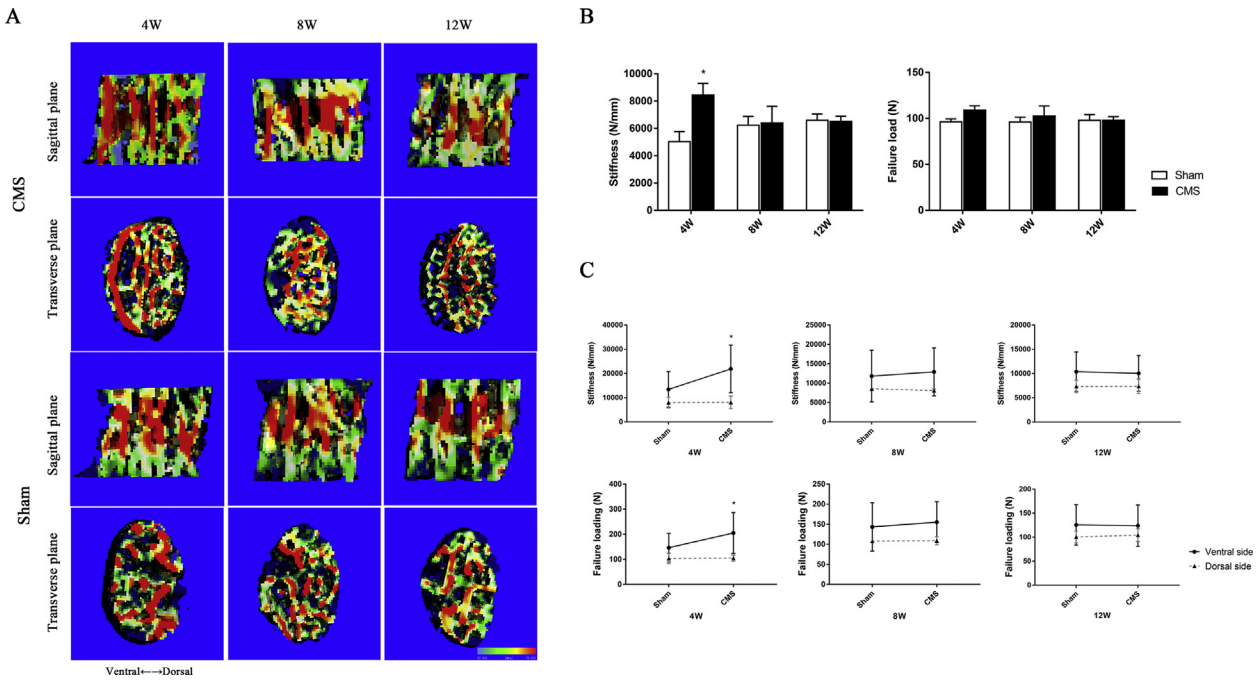

Figure 4. A-C) The cancellous bone biomechanical properties of the C6 vertebra by micro-FEA. (A) The stress distribution image of the C6 vertebral body in the midsagittal plane. The stress distribution transfer into the ventral side of the C6 vertebra from the middle part at 4 weeks after CMS. (B)The stiffness and failure load of the entire C6 vertebra. CMS significantly strengthened the biomechanics in the C6 vertebra at 4 weeks after surgery and showed no difference between the CMS and sham groups at 8 and 12 weeks. (C) The stiffness and failure load of the C6 vertebra in the ventral and dorsal sides. The CMS significantly increased the ventral side of biomechanical behaviours in the C6 vertebra at 4 weeks, while showed no effect on the dorsal side of the C6 vertebra. "*" indicated $P < 0.05$ compared with the sham group. micro-FEA = micro–finite element analysis; CMS =cervical muscle section.

vs. sham: 96.4 N vs. 108.9 N, P = 0.072) at 4 weeks. Whereas, the biomechanical properties of the C6 vertebral body showed no difference between groups at the time of 8 and 12 weeks (Figure 4B).

From the image of stress distribution, we found that the stress was mainly concentrated in the middle part of the vertebra in the sham group. On the contrary, the stress was transferred to the ventral side of the C6 vertebra at 4 weeks after CMS (Figure 4A). For further observation the biomechanics of ventral and dorsal sides of the C6 vertebra, we separately reconstructed the ventral and dorsal sides of C6 vertebra and analysed the stiffness and failure load, respectively. The results demonstrated that biomechanical behaviours of the ventral side of the C6 vertebra were significantly increased after CMS at 4 weeks (1.66 folds in stiffness and 1.36 folds in failure load), but showed no difference between groups in the dorsal side (Figure 4C).

CMS causes VEP defect earlier and calcification later

Evaluation of the axial view of the C6 caudal and C7 cranial endplates indicated that the VEL appeared in the ventral side at 4 weeks after CMS surgery, and the lesions seemed larger at 8 and 12 weeks. In contrast to the CMS group, VEP in the sham group were nearly intact at 4 and 8 weeks and had slight erosion at 12 weeks (Figure 5A). The VEL of the ventral side was increased by 23.0%, 24.9%, and 24.6% in the C6 caudal endplate and by 23.8%, 27.7%, and 28.1% in C7 cranial endplate after CMS at 4, 8, and 12 weeks, respectively, while the dorsal side of the VEL showed no significant difference between the CMS and sham groups in either C6 or C7 at all time points (Figure 5B). Moreover, the VEV showed no difference between the CMS and sham groups at 4 and 8 weeks, but was significantly increased in C6 caudal endplate (CMS vs. sham: 1.43 mm^3 vs. 1.21 mm^3) after CMS at 12 weeks (Figure 5C).

Safranin O/fast green staining was used to observe morphological and endochondral ossification of the VEP. The results showed that defects of the VEP were observed in the ventral side in the CMS rats at 4 weeks. This was followed by endochondral ossification at 8 weeks after surgery, as indicated by increased green-stained bone matrix surrounding the cavities in the CMS group relative to the sham group. The extent of entochondrostosis became more severe at the time of 12 weeks (Figure 6A). Simultaneously, the VEP scores were significantly increased in the CMS rats compared with the sham rats at each time point, confirming VEP degeneration (Figure 6B). These results, combined with the micro-CT data, exhibited that the position of the VEL was consistent with the biomechanical changes, which was concentrated in the ventral side of the vertebra at 4 weeks after CMS.

We further found that the expression of pSmad2/3 was increased at 4 weeks after CMS surgery and further at 8 and 12 weeks compared with the sham group. TRAP-positive cells were noted at 8 weeks in the CMS group but rarely detected in the sham group at any time point. This suggests that osteoclast resorption activity was increased after spinal instability (Figure 6C and D).

CMS accelerates IVDD

Narrowed intervertebral disc space is a typical characteristic regarded as a gold standard of IVDD diagnosis. We used micro-CT to analyse the IDH in the C6/7 segment and found that it was significantly decreased at 8 and 12 weeks in the CMS group compared with the sham group (CMS vs. sham: 0.46 mm vs. 0.53 mm at 8 weeks and 0.43 mm vs. 0.51 mm at 12 weeks, respectively) (Figure 7B).

Histological results revealed that, in the sham group, the intervertebral disc was almost normal, the NP contained abundant notochordal cells and was surrounded by large zones of extracellular matrix, and the AF was well organised. On the other hand, in CMS rats, the NP was reduced in size, and the AF became disorganised and some with the presence of cracks (Figure 7A). The CMS group exhibited higher disc degeneration scores than that of the sham group at 4 weeks, and the scores increased further at 8 and 12 weeks (Figure 7C).

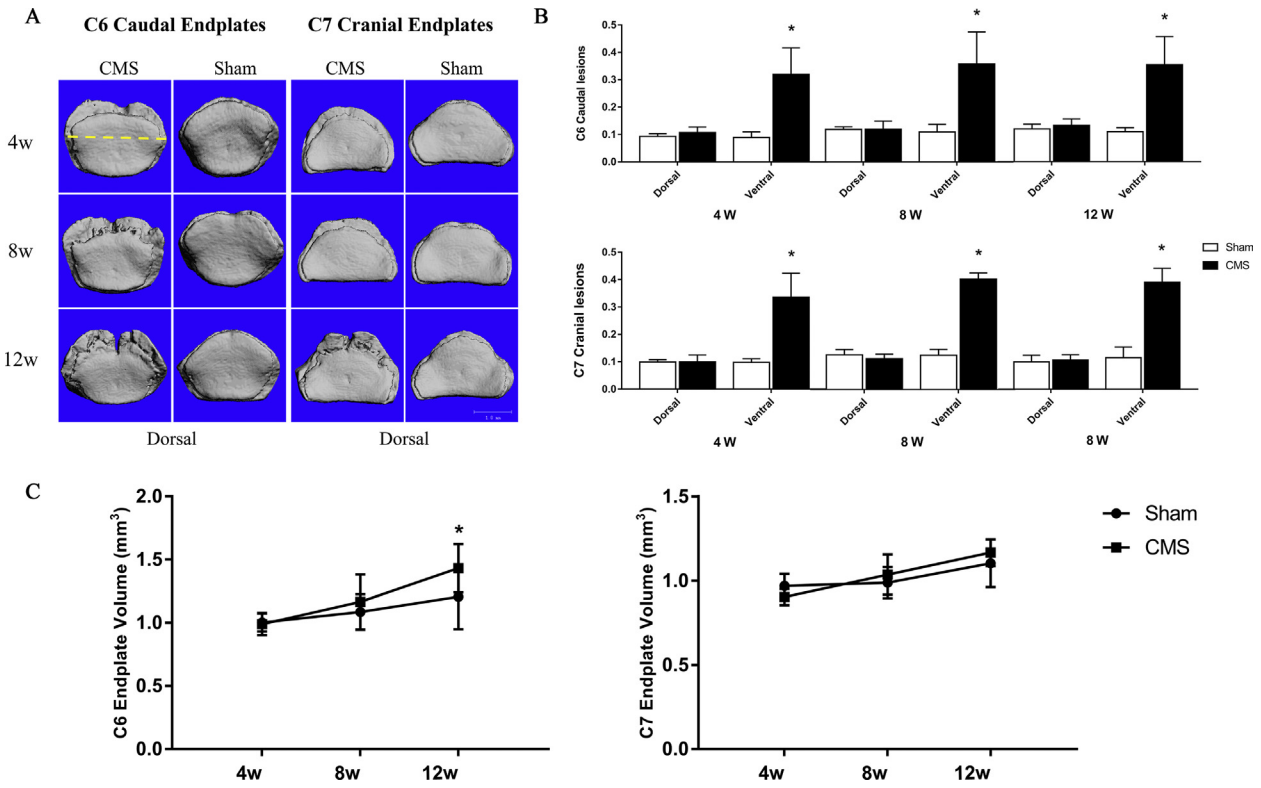

Figure 5. A-C) The changes of the vertebral endplate after CMS. (A) The axial view of the C6 caudal and C7 cranial endplate at 4, 8, and 12 weeks after surgery. The yellow dotted line means the midperpendicular of vertebral width of ventral to dorsal in the transverse plane to distinguish the ventral and dorsal side (showed in upper left corner image). (B) The VEL of C6/7 vertebral endplate in the ventral and dorsal sides between the CMS and sham groups at each time point. (C) The VEV of C6/7 vertebral endplate between the CMS and sham groups at each time point. "*" indicated $P < 0.05$ compared with the sham group. (For interpretation of the references to colour in this figure legend, the reader is referred to the Web version of this article.) CMS =cervical muscle section; VEL = vertebral endplate lesion; VEV = vertebral endplate volume.

Discussion

In this study, we revealed that instability of cervical spine induced by CMS caused bone formation in the ventral vertebra and significantly increased the biomechanical loading of the ventral side at the early stage. Meanwhile, early abrasion followed by calcification of the ventral side of VEP was evident, which was consistent with the enhanced biomechanical loading observed in the ventral vertebra. Consequently, the extent of VEP damage and IVDD was aggravated over time.

Mechanical loading is a particularly potent stimulus for bone formation, especially in the cancellous bone [21]. Bone mass is maintained by and adapted to mechanical strain, primarily as a result of muscular contraction [22,23]. *Morgan* et al. [24] found that cancellous bone loading *in vivo* increased bone density and bone volume fraction. Mechanical stimulation enhances the transformation of bone mesenchymal stem cells (BMSCs) toward osteoblastic lineage and stimulates BMSC proliferation [25]. The cervical spinal instability induced by facetectomy in our previous study significantly increased bone mass in vertebra at 12 weeks after surgery, indicating that instability of the spine may induce bone formation [17]. In normal condition, the mechanical loads of cervical spine induced by the weight of neck and head of rats were offset partly by contraction of the posterior musculatures. After transection of the posterior paraspinal musculatures, the stress distribution of cervical spine would transfer to the ventral side of vertebra and promote bone formation. Therefore, we separately measured the changes of bone microstructures in the ventral and dorsal vertebrae. The BV/TV of the ventral vertebra was increased by 22.9% after CMS surgery at 4 weeks, whereas bone mass of the dorsal side showed no difference between groups. Interestingly, the bone mass returned to the same level as the sham group at a later stage. The underlying reason may be that scar formation after surgery in the late phase restabilised the spine or that endplate and disc degeneration changed the biomechanics in the cervical spine, however further study is needed to clarify these postulations.

The biomechanical characteristics of the cervical spine between quadruped and bipedal might exist some differences. The quadruped spine is mainly loaded along its long axis (like the human spine), and it can be a valuable animal model for spine research [26]. *Griffin* et al. [27] observed the characteristics of the head and cervical vertebral column of rats, and they found that the rats have near vertical-orientated cervical vertebral columns but, in contrast to humans, they displace their head in space by movements at both the cervicothoracic junction and the craniocervical regions. To measure the mechanical properties of the mouse and rat disc in compression and torsion test, *Elliott* et al. [28] provided validation for the use of rodents as mechanical models of the human disc. The correlations of some lumbar spine properties with animal body weight further support the use of the lumbar spine in quadruped animals as appropriate mechanical models of the human lumbar spine. Therefore, the IVDD of rats can also simulate humans' to some extent.

As we expected, bone mass can also reflect biomechanical strength. There is a high correlation between the bone mineral parameters and the biomechanical properties [29]. CMS increased the bone mass of the C6 ventral vertebra at 4 weeks, which can infer that biomechanical properties of the ventral vertebra were also increased. Therefore, we estimated the vertebral biomechanical changes by micro-FEA and found that the stiffness and the failure load of the ventral side were significantly increased after CMS surgery in the early stage. In a normal cervical spine, the stress distribution of vertebra is mainly concentrated in the middle of the vertebral body. CMS surgery transferred the stress from the middle part of vertebra to the ventral side. This was consistent with bone mass changes in the vertebra.

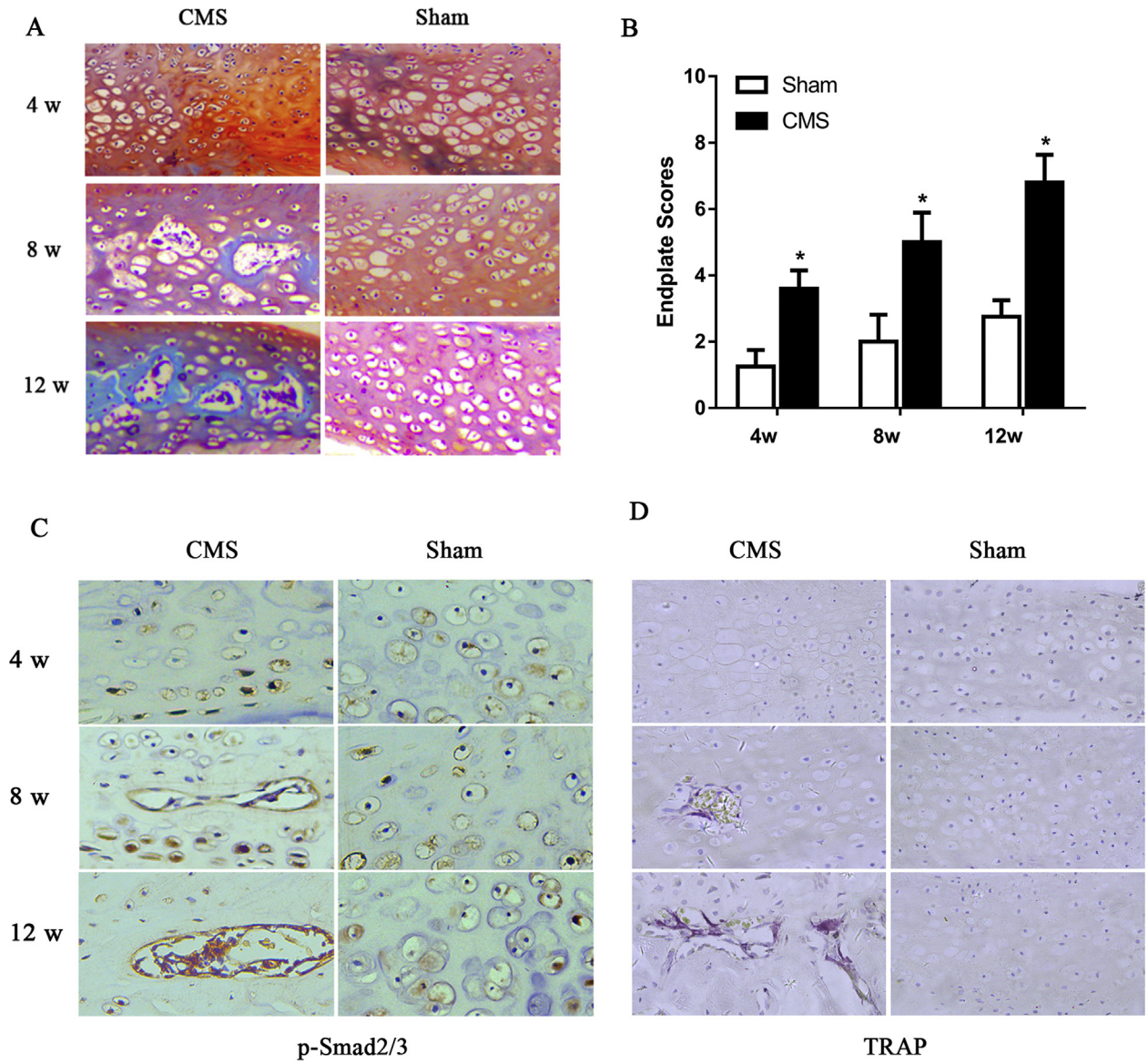

Figure 6. A-D) CMS initiated vertebral endplate damage in the C6/7 segment. (A) The safranine O/fast green staining of C6/7 vertebral endplates. (B) The histological grades evaluate between the CMS and sham groups at 4, 8, and 12 weeks. (C, D) Representative pSmad2/3 staining and TRAP staining of C6/7 vertebral endplates. "*" indicated $P < 0.05$ compared with the sham group. CMS = cervical muscle section; TRAP = tratrate resistant acid phosphatase.

As one of the functional structure of spinal unit, the VEP is greatly affected by biomechanical alterations. The physiological function of VEP is to help equalise loading between the intervertebral disc and vertebral body [30] and regulate metabolite transport between them [31]. Overload would cause endplate fracture and form abnormal stress distributions in the adjacent intervertebral disc and exhibit Modic's changes [32]. Cervicodorsal muscles and ligaments are critical in maintaining normal position and function of the cervical spine. By destroying both paraspinal muscles and posterior cervical spinal ligaments, *Wang* et al. [19] created a cervical spinal instability model in rats, which resulting in the loss of posterior column stability and IVDD. Our previous study demonstrated that VEL appeared on the ventral side in the CMS rats with the greater lesion at 12 weeks, followed by in situ calcification at 18 and 24 weeks [18]. In the previous study, we only observed the morphological change of the endplate at 12 weeks and later after CMS. Therefore, the present study further investigated VEL, together with the change in vertebral microarchitectures and biomechanical loading, at 4, 8, and 12 weeks after CMS. We found that the ventral side of the VEP was defected at 4 weeks, which was consistent with enhanced biomechanical loading in the ventral side. These results showed that initiation of the VEP damage might be caused by the augmentation of biomechanical loading in vertebra.

Regulation of bone formation and endochondral ossification were thought to be interrelated with TGF-β1 and Smad2/3 signalling pathway [33,34]. Prolonged and repeated upright posture upregulated TGF-β1, increased osteoblast number and function, and resulted in bone formation of the vertebra [16]. The present study displayed that CMS increased the expression of TGF-β1 and pSmad2/3 and promoted bone formation, and slightly decreased TRAP activities, in the early stage. Eventually, the bone resorption and formation reached a new balance through internal coupling mechanisms over time, with the bone mass and the trabecular structures showing no difference between groups.

Likewise, VEP degeneration is thought to begin with abnormal calcification, and the activation of pSmad2/3, which induces BMSCs transformation into osteoblasts, has been found to contribute to the pathogenesis of endochondral ossification in the endplate [33,35]. Alteration of the mechanical loading in the spine activates TGF-β1 signalling, which is associated with hypertrophy and calcification of the VEP [15,33]. In the present CMS animal model, we confirmed that spinal instability accelerated damage of the VEP and contributed to endplate

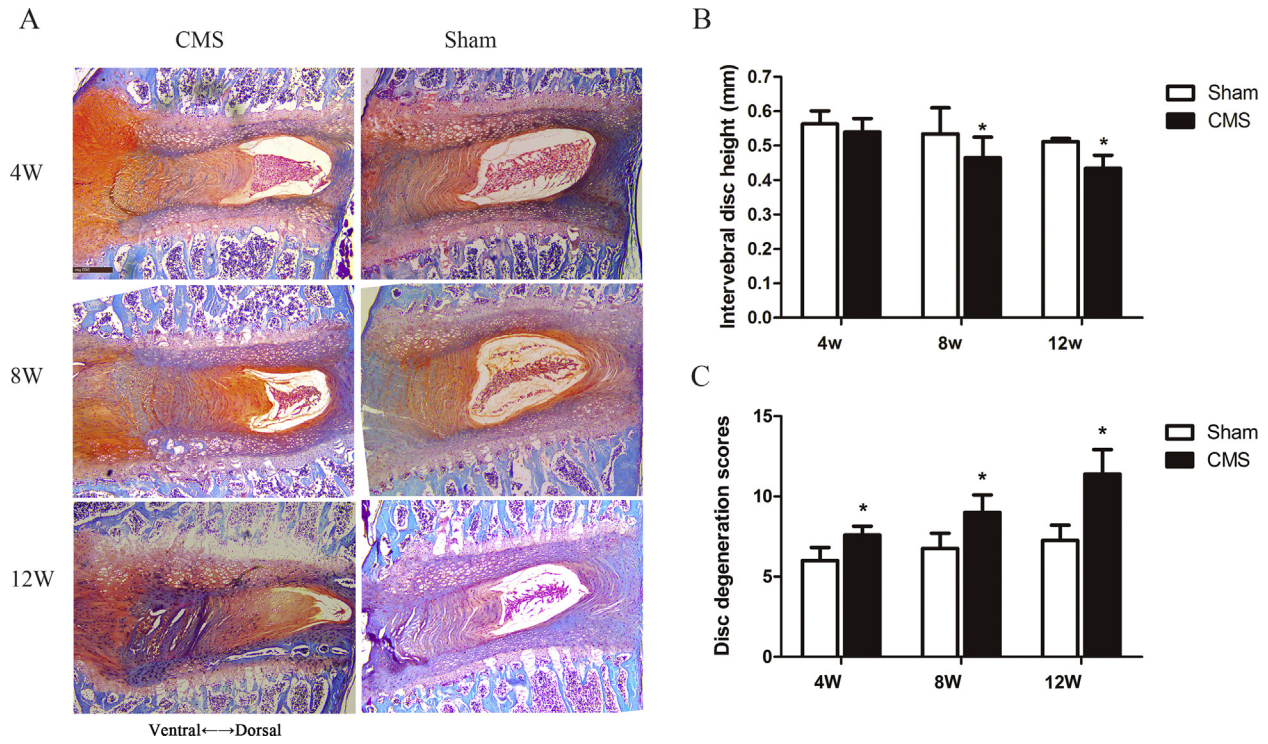

Figure 7. A-C) CMS-induced intervertebral disc degeneration of the C6/7 segment. (A) The safranine O/fast green staining of C6/7 disc tissues. (B, C) The histogram of intervertebral disc height and intervertebral disc degeneration scores between the CMS and sham groups at 4, 8, and 12 weeks. "*" indicated $P < 0.05$ compared with the sham group. CMS =cervical muscle section.

hypertrophy and sclerosis, at least part *via* the elevation of pSmad2/3 expression.

The VEP damage is one of the major initiating factors for the whole cascade of disc degeneration [36]. Damage of endplate decreases intradiscal pressure and increases the risk of disc degeneration [37]. In addition, the degeneration of VEP is thought to reduce nutrients transport from vertebral marrow to vertebral disc [38]. A large population-based sample confirmed that endplate defects are strongly and independently associated with disc degeneration [39]. VEP underwent defect earlier and followed by calcification later, and the endplate degeneration was aggravated over time in the CMS rats. Similarly, the IDH was continuously decreased and the IVDD score was also significantly increased in the CMS group than those in the sham group with time.

This study was first time to analyse the relationship between the spatiotemporal bone formation and biomechanical alteration in the vertebra with VEP damage and IVDD. However, there are still some limitations. Firstly, we have previously found that the degree of IVDD was gradually aggravated from C4/5 to C6/7. But, the present study was focused only on the C6/7 segment after CMS. Secondly, direct biomechanical testing of the bone undoubtedly provides more real information about mechanical integrity than FEA. However, the technique to distinguish the ventral and dorsal sides was very difficult to execute. Moreover, the present study exhibited a phenomenon that bone remodelling was rebalanced over time, while the VEP lesion and IVDD became more severe. The underlying mechanisms are unclear and further study is warranted.

Conclusion

The present study indicates that cervical spine instability caused by CMS induced bone formation and increased biomechanical loading in the ventral side of the vertebra at an early stage. The changes of biomechanical loading distribution might initiate VEP damage and IVDD.

Author contributions

Q.Z. and Q.L. designed the experiments. Q.L., Z.Y., Y.L., J.L., W.J., and Z.H. conducted the animal experiments. X.W., Z.H., and J.L. completed the data analysis. Q.L. wrote the manuscript, and Y.H. and Q.Z. revised the manuscript.

Conflict of interest

The authors have no conflicts of interest to disclose in relation to this article.

Acknowledgement

This study was supported by Guangdong Province Natural Science Foundation of China (No.2015A030313276) and Dean Foundation of Southern Medical University Nanfang Hospital (No.2016Z021).

References

[1] Raj PP. Intervertebral disc: anatomy-physiology-pathophysiology-treatment. Pain Pract 2008;8:18–44.
[2] Boos N, Weissbach S, Rohrbach H, Weiler C, Spratt KF, Nerlich AG. Classification of age-related changes in lumbar intervertebral discs: 2002 Volvo Award in basic science. Spine (Phila Pa 1976) 2002;27:2631–44.
[3] Miller JA, Schmatz C, Schultz AB. Lumbar disc degeneration: correlation with age, sex, and spine level in 600 autopsy specimens. Spine (Phila Pa 1976) 1998;13:173–8.
[4] Wang F, Cai F, Shi R, Wang XH, Wu XT. Aging and age related stresses: a senescence mechanism of intervertebral disc degeneration. Osteoarthr Cartil 2016;24:398–408.
[5] Hadjipavlou AG, Tzermiadianos MN, Bogduk N, Zindrick MR. The pathophysiology of disc degeneration: a critical review. J Bone Joint Surg Br 2008;90:1261–70.
[6] Smith LJ, Nerurkar NL, Choi KS, Harfe BD, Elliott DM. Degeneration and regeneration of the intervertebral disc: lessons from development. Dis Model Mech 2011;4:31–41.
[7] Fontana G, See E, Pandit A. Current trends in biologics delivery to restore intervertebral disc anabolism. Adv Drug Deliv Rev 2015;84:146–58.

[8] Paesold G, Nerlich AG, Boos N. Biological treatment strategies for disc degeneration: potentials and shortcomings. Eur Spine J 2008;16:447–68.
[9] Grunhagen T, Shirazi-Adl A, Fairbank JC, Urban JP. Intervertebral disk nutrition: a review of factors influencing concentrations of nutrients and metabolites. Orthop Clin N Am 2011;42:465–77.
[10] Madry H, van Dijk CN, Mueller-Gerbl M. The basic science of the subchondral bone. Knee Surg Sport Traumatol Arthrosc 2010;18:419–33.
[11] Stokes IA, Gardner-Morse M. Spinal stiffness increases with axial load: another stabilizing consequence of muscle action. J Electromyogr Kinesiol 2003;13:397–402.
[12] Peng B, Hao J, Hou S, Wu W, Jiang D, Fu X, et al. Possible pathogenesis of painful intervertebral disc degeneration. Spine (Phila Pa 1976) 2006;31:560–6.
[13] Mok FP, Samartzis D, Karppinen J, Luk KD, Fong DY, Cheung KM. ISSLS prize winner: prevalence, determinants, and association of Schmorl nodes of the lumbar spine with disc degeneration: a population-based study of 2449 individuals. Spine (Phila Pa 1976) 2010;35:1944–52.
[14] Bakker EW, Verhagen AP, van Trijffel E, Lucas C, Koes BW. Spinal mechanical load as a risk factor for low back pain: a systematic review of prospective cohort studies. Spine (Phila Pa 1976) 2009;34:E281–93.
[15] Bian Q, Liang QQ, Wan C, Hou W, Li CG, Zhao YJ, et al. Prolonged upright posture induces calcified hypertrophy in the cartilage end plate in rat lumbar spine. Spine (Phila Pa 1976) 2011;36:2011–20.
[16] Bian Q, Liang QQ, Hou W, Wan C, Li CG, Zhao YJ, et al. Prolonged and repeated upright posture promotes bone formation in rat lumbar vertebra. Spine (Phila Pa 1976) 2011;36:E380–7.
[17] Liu Q, Wang X, Hua Y, Kong G, Wu X, Huang Z, et al. Estrogen deficiency exacerbates intervertebral disc degeneration induced by spinal instability in rats. Spine (Phila Pa 1976) 2019;44:E510–5.
[18] Ding Y, Jiang J, Zhou J, Wu X, Huang Z, Chen J, et al. The effects of osteoporosis and disc degeneration on vertebral cartilage endplate lesions in rats. Eur Spine J 2014;23:1848–55.
[19] Wang YJ, Shi Q, Lu WW, Cheung KC, Darowish M, Li TF, et al. Cervical intervertebral disc degeneration induced by unbalanced dynamic and static forces: a novel in vivo rat model. Spine (Phila Pa 1976) 2006;31:1532–8.
[20] Han B, Zhu K, Li FC, Xiao YX, Feng J, Shi ZL, et al. A simple disc degeneration model induced by percutaneous needle puncture in the rat tail. Spine (Phila Pa 1976) 2008;33:1925–34.
[21] Lam H, Qin YX. The effects of frequency-dependent dynamic muscle stimulation on inhibition of trabecular bone loss in a disuse model. Bone 2008;43:1093–100.
[22] Pham MH, Buser Z, Wang JC, Acosta FL. Low-magnitude mechanical signals and the spine: a review of current and future applications. J Clin Neurosci 2017;40:18–23.
[23] Burr DB. Muscle strength, bone mass, and age-related bone loss. J Bone Miner Res 1997;12:1547–51.
[24] Morgan TG, Bostrom MP, van der Meulen MC. Tissue-level remodeling simulations of cancellous bone capture effects of in vivo loading in a rabbit model. J Biomech 2015;48:875–82.
[25] Thompson WR, Rubin CT, Rubin J. Mechanical regulation of signaling pathways in bone. Gene 2012;503:179–93.
[26] Smit TH. The use of a quadruped as an in vivo model for the study of the spine - biomechanical considerations. Eur Spine J 2002;11:137–44.
[27] Griffin C, Choong WY, Teh W, Buxton AJ, Bolton PS. Head and cervical spine posture in behaving rats: implications for modeling human conditions involving the head and cervical spine. Anat Rec (Hoboken) 2015;298:455–62. https://doi.org/10.1002/ar.23049*10.1002/ar.23049.
[28] Elliott DM, Sarver JJ. Young investigator award winner: validation of the mouse and rat disc as mechanical models of the human lumbar disc. Spine (Phila Pa 1976) 2004;29:713–22.
[29] Wright B, Ragan L, Niratisairak S, Hoiseth A, Stromsoe K, Steen H, et al. High correlation between mechanical properties and bone mineral parameters in embalmed femurs after long-term storage. Clin Biomech (Bristol, Avon) 2018;59:136–42.
[30] Setton LA, Zhu W, Weidenbaum M, Ratcliffe A, Mow VC. Compressive properties of the cartilaginous end-plate of the baboon lumbar spine. J Orthop Res 1993;11:228–39.
[31] Adams MA, Freeman BJ, Morrison HP, Nelson IW, Dolan P. Mechanical initiation of intervertebral disc degeneration. Spine (Phila Pa 1976) 2000;25:1625–36.
[32] Dolan P, Luo J, Pollintine P, Landham PR, Stefanakis M, Adams MA. Intervertebral disc decompression following endplate damage: implications for disc degeneration depend on spinal level and age. Spine (Phila Pa 1976) 2013;38:1473–81.
[33] Bian Q, Jain A, Xu X, Kebaish K, Crane JL, Zhang Z, et al. Excessive activation of TGFbeta by spinal instability causes vertebral endplate sclerosis. Sci Rep 2016;6:27093.
[34] Crane JL, Xian L, Cao X. Role of TGF-beta signaling in coupling bone remodeling. Methods Mol Biol 2016;1344:287–300.
[35] Roberts S, Urban JP, Evans H, Eisenstein SM. Transport properties of the human cartilage endplate in relation to its composition and calcification. Spine (Phila Pa 1976) 1996;21:415–20.
[36] Rade M, Maatta JH, Freidin MB, Airaksinen O, Karppinen J, Williams F. Vertebral endplate defect as initiating factor in intervertebral disc degeneration: strong association between endplate defect and disc degeneration in the general population. Spine (Phila Pa 1976) 2018;43:412–9.
[37] Holm S, Holm AK, Ekstrom L, Karladani A, Hansson T. Experimental disc degeneration due to endplate injury. J Spinal Disord Tech 2004;17:64–71.
[38] Moore RJ. The vertebral end-plate: what do we know? Eur Spine J 2000;9:92–6.
[39] Rade M, Maatta JH, Freidin MB, Airaksinen O, Karppinen J, Williams FM. Vertebral endplate defect as initiating factor in intervertebral disc degeneration; strong association between endplate defect and disc degeneration in the general population. Spine (Phila Pa 1976) 2018;43:412–9.